

Polyimide@Ketjenblack Composite: A Porous Organic Cathode for Fast Rechargeable Potassium-Ion Batteries

Chenglin Zhang, Yang Xu, Kaiming He, Yulian Dong, Huaping Zhao, Lukas Medenbach, Yuhan Wu, Andrea Balducci, Thomas Hannappel, and Yong Lei*

Potassium-ion batteries (PIBs) configured by organic electrodes have been identified as a promising alternative to lithium-ion batteries. Here, a porous organic Polyimide@Ketjenblack is demonstrated in PIBs as a cathode, which exhibits excellent performance with a large reversible capacity (143 mAh g⁻¹ at 100 mA g⁻¹), high rate capability (125 and 105 mAh g⁻¹ at 1000 and 5000 mA g⁻¹), and long cycling stability (76% capacity retention at 2000 mA g⁻¹ over 1000 cycles). The domination of fast capacitive-like reaction kinetics is verified, which benefits from the porous structure synthesized using in situ polymerization. Moreover, a renewable and low-cost full cell is demonstrated with superior rate behavior (106 mAh g⁻¹ at 3200 mA g⁻¹). This work proposes a strategy to design polymer electrodes for high-performance organic PIBs.

earth abundance of K (almost 1000 times more than Li) and the similar electrochemical properties to Li-ion batteries. Compared with well-studied sodium-ion batteries (SIBs), K has comparable resource reserves but a much closer standard electrode potential to Li (-2.71 V for Na/Na⁺, -2.93 V for K/K⁺, and -3.04 V for Li/Li⁺, versus standard hydrogen electrode), implying that a similar voltage window and energy density to those of LIBs might be achieved in PIBs. Therefore, the PIB could be a desirable alternative of LIBs.^[3-6] Unfortunately, most conventional inorganic cathodes that have been widely demonstrated in LIBs and SIBs exhibit

1. Introduction

With the increasing demand for lithium-ion batteries (LIBs) used in portable electronic devices and electronic vehicles, the concern of limited lithium resources has attracted more and more attention, hence low-cost energy storage technologies need to be explored and commercialized.^[1,2] Recently, potassium-ion batteries (PIBs) came in our sight due to the

unsatisfactory electrochemical performance in PIBs, resulting from the large size of K-ions (1.38 Å) and kinetic diffusion limitations in the bulk-phase of inorganic cathodes.^[7-19]

Compared to inorganic cathode materials, organic and polymer materials possess flexible molecular structures that could be better host materials for K-ions.^[20-24] Organic materials have been widely investigated as electrodes in LIBs and SIBs.^[19,20,25-28] However, suffering from poor conductivity, low active-site exposure, and easy solubility of organic materials, the electron transport, ion diffusion, and stability of organic electrodes are commonly depressed.^[29-35] Hence the research progress so far for improving the rate capability and the cyclability of organic cathodes in PIBs are highly unfavorable. Exploring strategies to promote the conductivity, activity, and stability of organic materials is urgently needed. And fabricating electrodes for PIBs composed of stable polymers and carbon additives, especially with heterogeneous structures, could be an effective approach. Based on this recognition, our strategy is the development of a stable porous polymer@carbon composite cathode for realizing a high-performance potassium-organic battery. The porous structure of a polymer-coated carbon skeleton can not only increase the conductivity of the cathode, but also avoids the self-stacking of polymers, leading to an enhanced charge-carrier mobility and more exposed active sites for achieving a high rate capability. Besides, the solubility of the polymer is much lower than that of the monomer, which can effectively improve the stability of the cathode.


In this work, a fast-rechargeable potassium-ion battery was first demonstrated using a porous Polyimide@Ketjenblack (PIM@KB) as the cathode. This porous composite was synthesized through in situ polymerization of 1,4,5,8-naphthalenetetracarboxylic dianhydride (NTCDA) monomers on Ketjenblack.

C. Zhang, Dr. Y. Xu, Dr. H. Zhao, Y. Wu, Prof. T. Hannappel, Prof. Y. Lei
Institute of Physics and IMN MacroNano@
Technical University of Ilmenau
Ilmenau 98693, Germany
E-mail: yong.lei@tu-ilmenau.de

Dr. Y. Xu
Department of Chemistry
University College London
London WC1H 0AJ, UK

K. He, Y. Dong
Institute of Nanochemistry and Nanobiology
Shanghai University
Shanghai 200444, China

Dr. L. Medenbach, Prof. A. Balducci
Institute for Technical Chemistry and Environmental Chemistry
Friedrich-Schiller-University Jena
Philosophenweg 7a, Jena 07743, Germany

 The ORCID identification number(s) for the author(s) of this article can be found under <https://doi.org/10.1002/smll.202002953>.

© 2020 The Authors. Published by Wiley-VCH GmbH. This is an open access article under the terms of the Creative Commons Attribution License, which permits use, distribution and reproduction in any medium, provided the original work is properly cited.

DOI: 10.1002/smll.202002953

In particular, such a porous composite exhibited a high reversible capacity (143 mAh g^{-1} at 100 mA g^{-1} , Coulombic efficiency: almost 100%), superior rate capability (125 and 105 mAh g^{-1} at 1000 and 5000 mA g^{-1}), and cyclability (capacity retained 76% after 1000 cycles at 2000 mA g^{-1}). Additionally, the wetting time of the composite was highly shortened, leading to a much better self-improving ability. The study of organic materials compositions and electrochemical mechanisms revealed that both the porous structure and the improved conductivity are the keys to the enhanced K-ion transport and diffusion, which enables the fast-rechargeable capability. Besides, an ultrafast rechargeable full cell was also configured by using the PIM@KB cathode with a nitrogen-doped soft carbon anode.

2. Results and Discussion

The overall chemical and structural fabrication processes of the porous PIM@KB composite are illustrated in **Figure 1a** and **Figure S1** (Supporting Information). In brief, a homogeneous suspension of Ketjenblack and NTCDA was first prepared in a *N*-Methyl-2-pyrrolidone (NMP) solvent, making sure that Ketjenblack was completely wet. Then, a stoichiometric amount of 1,2-diaminoethane (EDA) was added

to the suspension. During the polymerization reaction, the PIM polymer was directly deposited on the surface of the self-aggregated porous Ketjenblack. Consequently, with the polymer condensation, the porous PIM@KB composite has been obtained (all details of the fabrication process are given in the Experimental Section). The color of the as-prepared PIM is orange while the PIM@KB composite is black (**Figure S2**, Supporting Information). **Figure 1b,c** is scanning electron microscopy (SEM) images of PIM and PIM@KB composite, showing a clear morphology difference of the two samples. PIM@KB has a morphology as wrinkled particles overspread the sample surfaces. SEM images at high magnification (**Figure 1d**; **Figures S3** and **S4**, Supporting Information) demonstrate a porous structure of PIM@KB. From transmission electron microscopy (TEM) measurements, the strong and distinct difference of the contrast distribution of PIM@KB (**Figure 1f**) compared to that of PIM (**Figure 1e**) suggests the porous structure of the composite as well, implying that the PIM does not completely fill the empty space within the carbon skeleton. To further clarify the porous structure, we conducted N_2 -physisorption measurements for PIM@KB and PIM samples. The nitrogen adsorption–desorption isotherms in **Figure 1g** reveal that the Brunauer–Emmett–Teller (BET) surface areas of PIM@KB and PIM are 82.6 and $18.7 \text{ m}^2 \text{ g}^{-1}$,

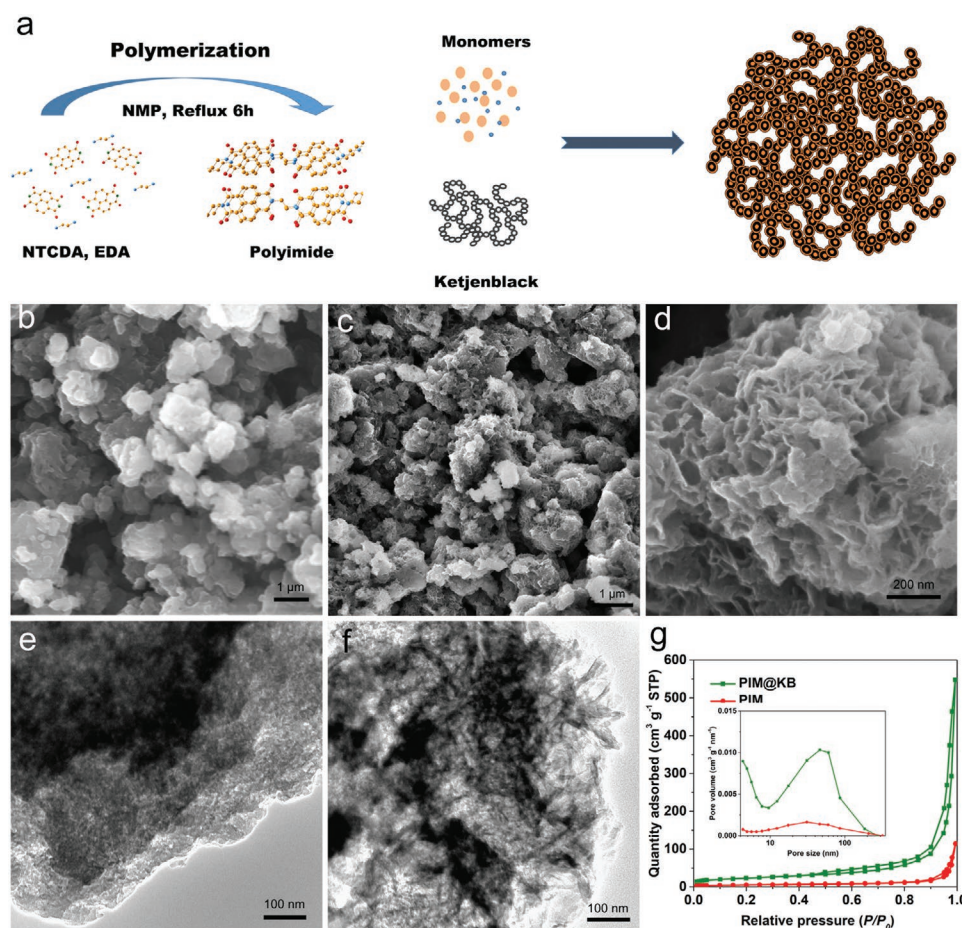


Figure 1. Materials preparation, structural and compositional information. a) Illustration of PIM@KB synthesis. SEM images of b) PIM and c,d) PIM@KB. TEM images of e) PIM and f) PIM@KB. g) Nitrogen adsorption–desorption isotherms (inset shows the related pore-size distribution).

respectively. PIM@KB exhibits type IV isotherms with H3 hysteresis loops, suggesting a meso/macroporous structure. The pore-size distribution of both samples was evaluated by Barrett–Joyner–Halenda (BJH) model, it demonstrates the mesopores (≈ 4 nm) and macropores (≈ 50 nm) both exist in PIM@KB. The mesopores and macropores are mainly generated from Ketjenblack component and the composite construction, respectively, which agrees with the SEM and TEM results. This type of structure ensures an effective contact between the electrolyte and the active materials, which is the key for the high (ionic transport) kinetics when using it as PIB cathode. In addition, Fourier transform infrared (FTIR) spectroscopy (Figure S5, Supporting Information) was employed to verify the chemical components of the samples. The absorption peaks at 1770, 1656, and 1350 cm^{-1} are attributed to the asymmetric and symmetric stretching vibrations of the C=O and the symmetric

stretching vibrations of $-\text{C}-\text{N}-\text{C}-$ bond in the PIM units, respectively.^[36] These peaks can be found in both contrast samples, suggesting the existence of the PIM in the composite.

To evaluate the electrochemical performance of the PIM@KB composite, a contrast experiment was conducted for the comparison with bare PIM. A half-cell was configured using the organic cathode against a potassium metal anode. As shown in **Figure 2a**, the typical cyclic voltammetry (CV) curves from the second cycles of PIM@KB and bare PIM display two similar pairs of reversible redox peaks with anodic potentials located at about 2.4, 2.9 V versus K/K^+ and the cathodic potentials located at about 1.8, 2.25 V versus K/K^+ , respectively. Obviously, it demonstrates a similar electrochemistry for both cathodes, and two carbonyl groups in each PIM unit perform electrochemical redox reactions. A similar behavior can be found in Li-ion and Na-ion batteries.^[36–41] Additionally, the different capacities

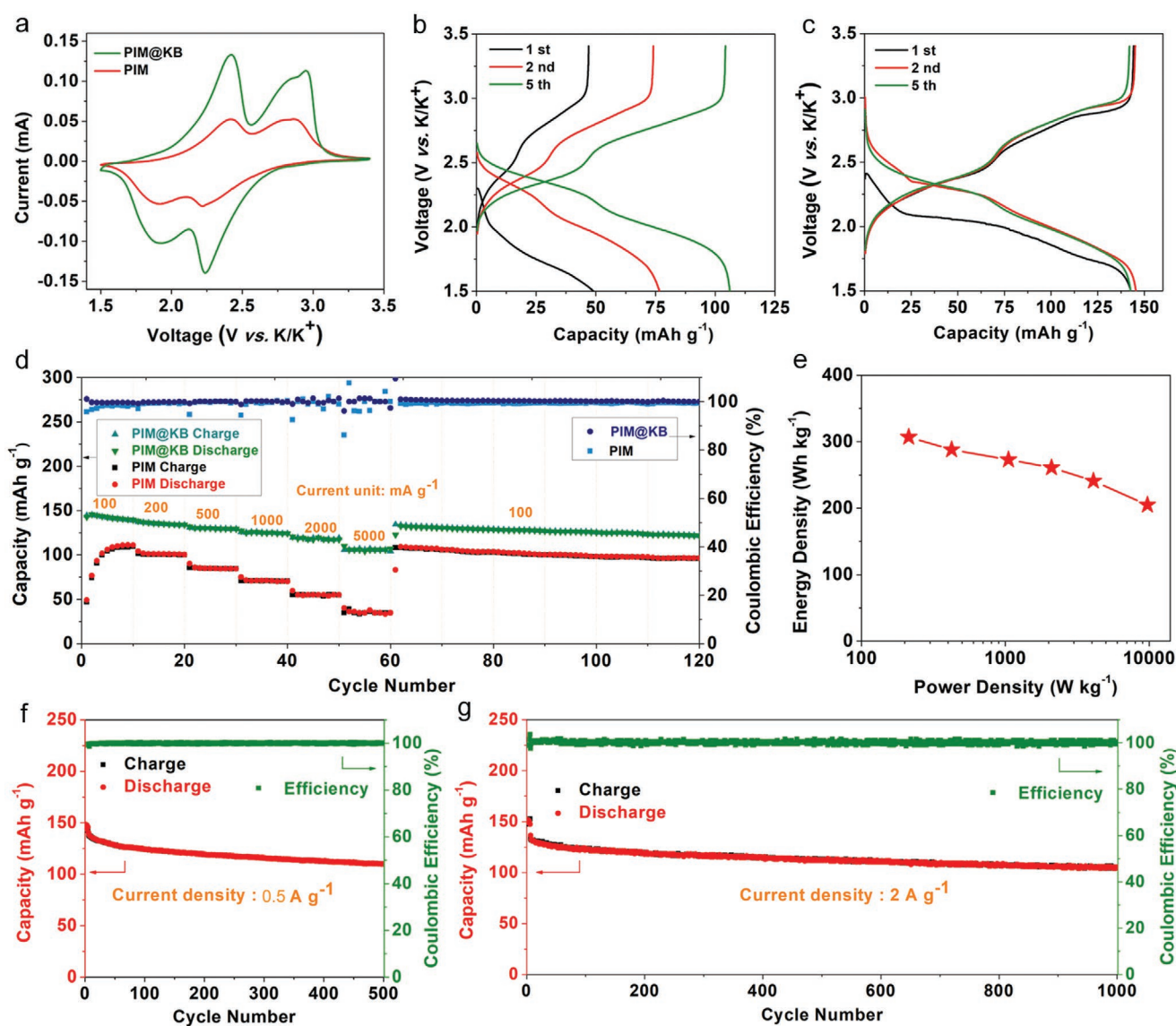


Figure 2. Electrochemical behavior of PIM electrodes. a) CV curves at scan rate of 0.2 mV s^{-1} . Initial discharge and charge profiles of b) PIM and c) PIM@KB at current density of 100 mA g^{-1} . d) Rate performance of various current densities. e) Ragone plot of PIM@KB. Cycling performance of PIM@KB at different current densities of f) 0.5 and g) 2 A g^{-1} .

were clearly observed for two different samples, which were in accordance with their initial ability of K-ion storage. Therefore, the voltage profiles from the starting cycles were further analyzed. As shown in Figure 2b,c, the PIM exhibits reversible capacities of 49, 76, and 115 mAh g⁻¹ during the first, the second, and the fifth cycles, respectively, which indicates a long wetting time for the PIM sample. On the contrary, the PIM@KB exhibits very close capacities during the initial cycles, suggesting it possesses an excellent self-improving ability. Such an advantage shall benefit from the porous structure of PIM@KB. As illustrated in Figure S6 (Supporting Information), the organic electrode with porous structure has much shorter ion-diffusion pathways than the electrode with bulk structure. As a result, the porous organic electrode allows K ions to easily approach to all active sites, enabling all the active materials to efficiently react with K ions. In addition, the second charge and discharge profiles are in a close correspondence with the CV results and show approximate voltage plateaus corresponding to the anodic and cathodic peaks. The first charge and discharge capacities of the PIM@KB electrode are 144 and 146 mAh g⁻¹ at a current density of 100 mA g⁻¹, corresponding to an initial columbic efficiency of 99%, which is even higher than those of the most inorganic K-ion cathodes. The reversible capacity is 77% of the theoretically calculated capacity (183 mAh g⁻¹) of its analogue, which corresponds to 1.6-electron transportation per PIM unit. In principle, each PIM unit has four carbonyl groups, which should be able to transfer 4-electrons for enolization with four K-ions. Unfortunately, like in Li-ion and Na-ion batteries, the charge and discharge reactions of PIM in K-ion batteries just take place on two carbonyl groups.^[40] Besides, a much better rate capability of PIM@KB electrode compared with bare PIM electrode was also demonstrated. As shown in Figure 2d, the PIM@KB electrode exhibits superior rate performance with capacities of 143, 135, 130, 125, 118, and 105 mAh g⁻¹ at various rates of 100, 200, 500, 1000, 2000, and 5000 mA g⁻¹, respectively, and when the current density returns to 100 mA g⁻¹, the capacity is recovered to 143 mAh g⁻¹ and is maintained for about 85% after further 60 cycles. Table S1 (Supporting Information) shows that the electrochemical performance of PIM@KB is highly competitive among reported organic cathodes for PIBs. The discharge and charge profiles (Figures S7 and S8, Supporting Information) show that PIM@KB possesses a smaller polarization at various rates than that of PIM, which shall benefit from the improved conductivity of the PIM/KB composite. Thus, as compared to the much lower rate performance of the bare PIM, the improved conductivity and the porous self-stacking structure of PIM@KB facilitate electron transport and K-ion diffusion, which are the crucial roles for the excellent rate capability of PIM@KB. It is worth noting that PIM@KB can maintain a high energy density with increasing power density, and even at an ultrahigh power density of 9715 W kg⁻¹, it can still achieve a high energy density of 205 Wh kg⁻¹ (Figure 2e and Figure S9 (Supporting Information), all the energy densities and power densities are calculated based on cathode materials). Such high energy density and power density performance is very competitive among almost all cathodes previously reported in PIBs.^[8,33] Moreover, PIM@KB also shows an outstanding long-term cycling stability. As shown in Figure 2f,g, PIM@KB can deliver capacities

of 110 mAh g⁻¹ at 0.5 A g⁻¹ after 500 cycles and 105 mAh g⁻¹ at 2.0 A g⁻¹ after 1000 cycles, and the charge and discharge plateau can still be observed (Figure S10, Supporting Information), which benefits from the facile and stable electrochemical redox reactions that occur on the porous composite.

To further understand the responsible redox reactions between carbonyl and K-ions, the changes in bonding state and lattice structure are investigated and discussed by the characterization of FTIR and X-ray diffraction (XRD) spectroscopy. In principle, each PIM unit has four carbonyl groups, which should be able to transfer 4-electrons for enolization with four K-ions. Unfortunately, like that in Li- and Na-ion batteries, the charge and discharge reactions of PIM in K-ion batteries just take place on two carbonyl groups (Figure 3a).^[40] Figure 3b shows different selected charge and discharge states for the in situ characterization. As shown in Figure 3c, two main peaks including, C–N and C–O–K are detected, corresponding to the wavenumber of about 1150, 1350, and 1623 cm⁻¹, respectively.^[36,38] During the discharge process, the intensities of the C–O–K peak and the C–O peak increase, meaning that the oxygen coordinates with K-ions, when the reduction reaction happens. During the charge process, the intensities of both FTIR peaks decrease, indicating that the K-ions extraction from the electrode occurs when the oxidation reaction happens. Meanwhile, the intensity changes of the C–N peaks are consistent with the changes of the charge and discharge states, which is consistent with changes of the conjugate environments, when the reduction and oxidation reactions happen.^[38,40] Moreover, the C–N peaks for all charge and discharge states obviously shift compared to that of the pristine PIM@KB electrode without K-ion insertion and extraction. The reason should be attributed to that the chemical bonds of perylene units on the polymer chains are rigid, while the C–N bonds connecting perylene units are flexible. After the insertion and extraction of K ions, the polymer molecular chains have been rearranged, leading to the shift of rotatable C–N peaks. Figure 3d shows the XRD patterns of three critical states during the charge and discharge process, which reveals that the change of the PIM@KB lattice structure accompanies with K-ion insertion and extraction. The (122) peak at about 25.1° is the main plane of the layer polymer structure (Figure S11 in the Supporting Information shows the peak of the carbon complex on Al foil is almost invisible). It obviously shifts to low-angle directions after full discharging, indicating increased distance between the main planes, which is attributed to the insertion of K-ion. Subsequently, the (122) peak recovers to its original position, meaning the distance decreases due to the extraction of K-ions.^[38] Moreover, the indistinctive change between the full charge state and the pristine state suggests that this kind of flexible organic polymer exhibits a negligible structure damage after K-ion insertion and extraction. In addition, as shown in Figure S12a,b (Supporting Information), the porous structure of PIM@KB is well preserved after 100 cycles. Overall, the facile reversible redox reaction and structural stability of the PIM@KB cathode are confirmed.

The fast reaction kinetics of PIM@KB was investigated using CV at different scan rates from 0.2 to 10 mV s⁻¹. As shown in Figure 4a, the anodic peaks (A1 and A2) and cathodic peaks (C1 and C2) at different scan rates are clearly observed, which

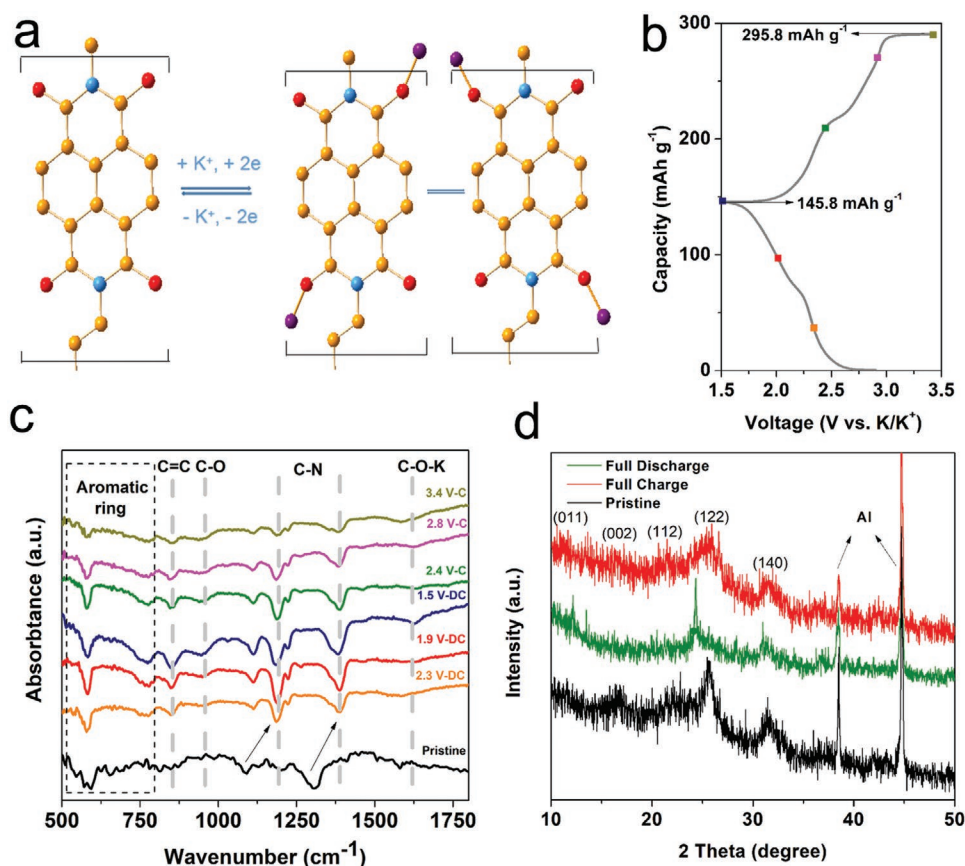


Figure 3. Investigation of the electrochemical mechanism. a) Illustration of chemical reaction. b) Indication of different discharge and charge states for PIM@KB. c) FTIR spectra and d) XRD patterns of PIM@KB at different states.

means two pairs of redox reaction process occur at comparable high scan rates. Moreover, the broad peaks imply that the pseudo-capacitive reaction might be the main K-ion storage route. Figure 4b shows the peak currents at different scan rates from the rate CV results. The anodic peaks and cathodic peaks are nearly the same and the current ratio is close to 1, which could be the result of a fast kinetics with the participation of a capacitive-like reaction.^[41,42] Further analysis was conducted to determine the contribution of the capacitive-like reaction by using the following equation

$$i = av^b \quad (1)$$

for a redox reaction, the measured peak current (i) at a fixed voltage obeys a power-law relationship with the voltage sweep scan rate (v). Figure 4c shows the plot of $\log(i)$ versus $\log(v)$, which can be used to calculate the b -value. As we know, a b -value of 0.5 corresponds to an ideal intercalation reaction process and a b -value of 1 corresponds to an ideal capacitive reaction process.^[41–44] Here, the different b -values corresponding to anodic and cathodic peak currents (A1, A2, C1, and C2) were estimated to be about 0.94, 0.93, 0.83, 0.86, respectively, implying that a significant portion of the capacitive-like ion storage reaction dominates. This kind of surface-controlled characteristic enables a supercapacitor-like high-rate electrochemical behavior. Moreover, we evaluated the level of

the capacitive-like domination using the relation of current response, i , with a combination of capacitor-like response (k_1v) and diffusion response ($k_2v^{1/2}$)

$$i = k_1v + k_2v^{1/2} \quad (2)$$

By calculating the k_1 and k_2 constants, the capacitive-like domination can be determined. As shown in Figure 4d, the surface-controlled capacity is about 66% at a high scan rate of 2.0 mV s⁻¹. Therefore, the high power density and the energy density of PIM@KB should be rendered by the unique porous morphology and high conductivity of the composite, which effectively shortens the K-ion diffusion distances and accelerates the redox reactions. Additionally, the accelerating reaction kinetics was demonstrated by using electrochemical impedance spectroscopic (EIS) measurement. As shown in Figure S13 (Supporting Information), the interface resistance of PIM@KB represented by semicircles is smaller than that of PIM, suggesting that the porous structure constructed with the carbon skeleton shows an advantage of fast interface charge transfer. The overpotential and equilibrium potential of PIM@KB and bare PIM were also evaluated using galvanostatic intermittent titration technique (GITT) measurements. As shown in Figure S14 (Supporting Information), the overpotentials of PIM@KB are lower than those of PIM during two main discharge plateaus. Both EIS and GITT investigations further validate the

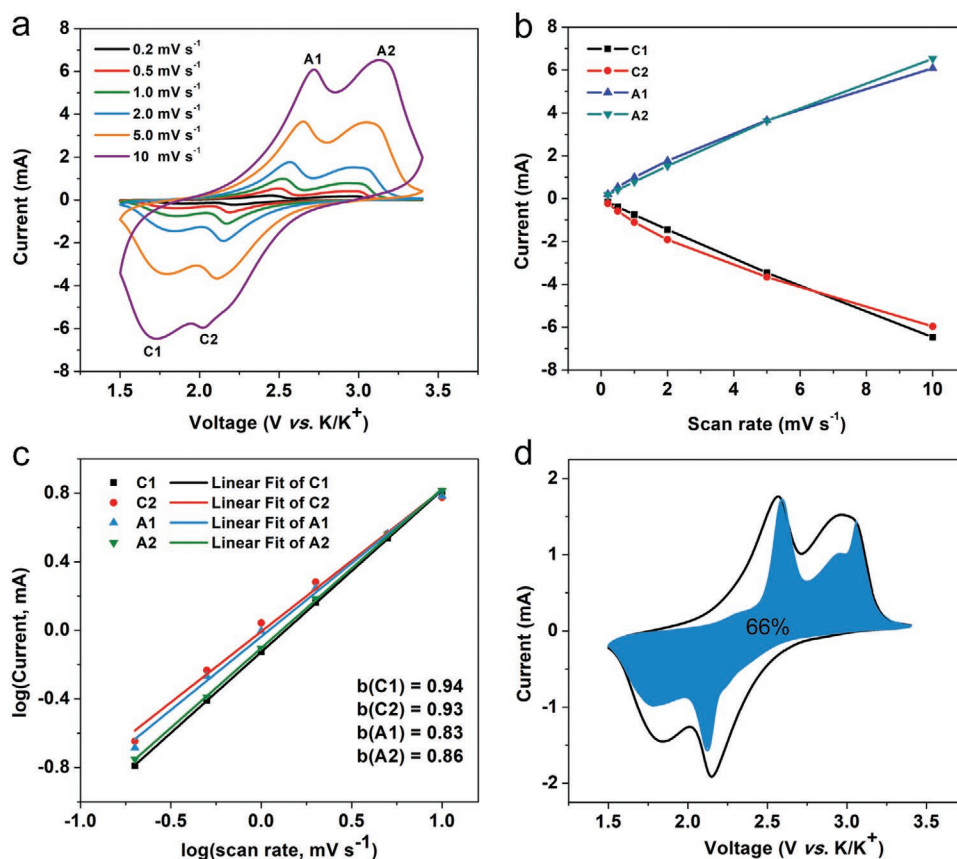


Figure 4. Kinetics and quantitative mechanism analysis. a) CV curves of PIM@KB at various scan rates. b) Linear relationship between the peak current and scan rate. c) Determination of *b*-value using the relationship between the peak current and scan rate. d) Capacitive-controlled contribution to charge storage of PIM@KB scan rate of 2.0 mV s⁻¹.

fast redox reaction that enables the high rate performance of porous PIM@KB.

Inspired by the excellent electrochemical behavior of the PIM@KB in half cells, we assembled a full cell by using the PIM@KB cathode against a nitrogen-doped soft carbon anode, and further evaluated the commercial application potential of this organic cathode. The nitrogen-doped soft carbon anode was prepared according to our previous work and was prepotassiated before assembling the full cell.^[44] The rate performance of the full cell (Figure 5a) exhibited reversible capacities of 139, 131, 125, 115, and 106 mAh g⁻¹ at different rates of 200, 400, 800, 1600, and 3200 mA g⁻¹, respectively. The Coulombic efficiency keeps almost 100% during the various charge and discharge rates. Remarkably, the energy and power densities of PIM@KB/soft carbon are one of the best ones among all representative potassium-ion full batteries. (Figure S15, Supporting Information).^[8,10,15,33,44–48] Figure 5b displays the charge and discharge profiles at different rates. As compared with the profiles in half cells, the main charge and discharge plateaus fall by about 0.5 V due to the comparatively high charge and discharge plateaus of the anode. The cycling stability was also investigated, which exhibits a capacity of 102 mAh g⁻¹ at 800 mA g⁻¹ over 30 cycles (Figure 5c). It is worth noting that the working time of one cycle only needs about 16 min (Figure 5d), which is even competitive with the working time of some ion storage capacitors.^[49–51]

3. Conclusions

In summary, a porous Polyimide@Ketjenblack composite was first demonstrated as an organic cathode for ultrafast and durable potassium-ion batteries, which can deliver a capacity of 143, 105 mAh g⁻¹ at 100 and 5000 mA g⁻¹, respectively, and can possess a reversible capacity of 105 mAh g⁻¹ over 1000 cycles at 2 A g⁻¹. The porous organic composite was synthesized using an in situ polymerization, which is proposed as an efficient approach to enhance electrochemical performance of PIB organic cathodes. We also found that the redox reaction kinetics of the K-ion storage shows a capacitive-like property that is attributed to facile charge diffusion and electron transport with this porous composite. Furthermore, the possibility to realize a full potassium-ion battery with superior rate capability was demonstrated, which exhibits a capacity of 106 mAh g⁻¹ at a high current density of 3200 mA g⁻¹. This work provides a way to design polymer electrodes for potassium-ion batteries with high capacity and rate capability.

4. Experimental Section

Materials Synthesis: The PIM@KB composite was prepared by an in situ polymerization process. In a typical process, 50 mg Ketjenblack

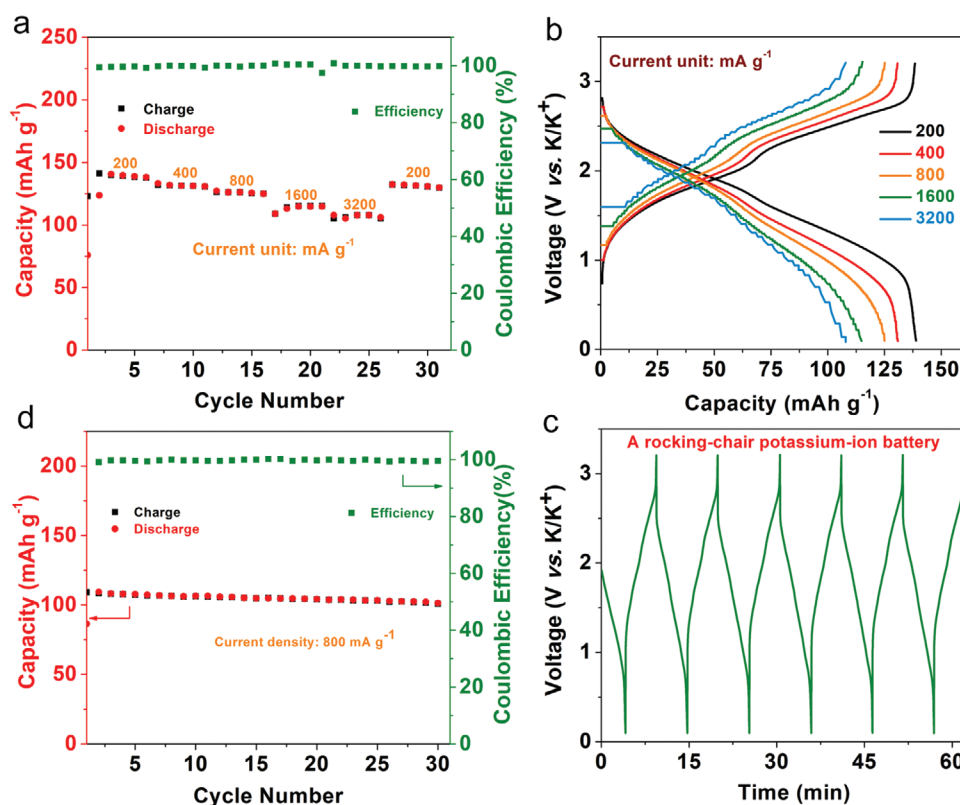


Figure 5. Performance of the full battery. a) Rate performance and discharge and b) charge profiles of the PIM@KB//NC full cell at various current densities. c) Cycling performance and d) working time of the full cell at current density of 800 mA g⁻¹.

was dispersed in 25 mL NMP (1.033 g cm⁻³) in a round flask and stirred at room temperature for 1 h. After a homogeneous suspension had completely been formed, 268 mg NTCDA (≥97%) and the stoichiometric EDA (≥99%) were then respectively added into the suspension and refluxed in an oil bath for 6 h under vigorous stirring. Finally, a back precipitate was collected by filtration, and washed with deionized water three times. The orange bare polyimide was prepared using the same procedure without Ketjenblack.

Materials Characterizations: The structure and morphology of the samples were observed by SEM and TEM. SEM was performed on a Hitachi 434 S4800, and TEM was performed on a JEOL JEM-435 2100F. FTIR spectra were performed on an AVATAR 370. XRD patterns were identified using an 18 KW D/MAX2500V PC diffractometer at a scan rate of 2° min⁻¹. The N₂-physiosorption measurements were conducted using Quantachrome ASiQwin- automated gas sorption analyzer.

Electrochemical Measurements: The PIM@KB electrodes were prepared by mixing 80 wt% as-synthesized active composites, 10 wt% super P and 10 wt% sodium salt of carboxymethyl ether of cellulose (CMC). The bare PIM electrodes were prepared by mixing 60 wt% pure PIM, 30 wt% super P, and 10 wt% CMC. Deionized water was used as the solvent to grind the mixture into a slurry. Then, the slurry was coated on an Al foil by using the doctor-blade, and the mass loading of the active materials was controlled to about 1.5 mg cm⁻². The coin-cell configuration (CR 2032) was assembled in an N₂-filled glove box. The electrolyte was prepared by mixing 1.0 M potassium bis(fluorosulfonyl)imide (KFSI) in ethylene carbonate and diethyl carbonate (vol, EC: DEC = 1:1) in an N₂-filled glove box. The separator was a glass microfiber filter (Whatman, Grade GF/B). CV, GITT, and EIS tests were performed on a VSP electrochemical workstation (Bio-Logic, France). Galvanostatic charge/discharge tests were performed on a Land CT 2001A 449 battery testing system (Land, China). Nitrogen-doped carbon electrodes that were prepared according to our previous work were used as anodes to assemble the full cells.^[44] The anodes were prepotassiated by cycling in half cells.

Supporting Information

Supporting Information is available from the Wiley Online Library or from the author.

Acknowledgements

This work was financially supported by the German Research Foundation (DFG: LE2249/5-1), C.Z. is sponsored by the China Scholarship Council. The authors thank Dr. Jörg Pezoldt for the help with FTIR measurement. Open access funding enabled and organized by Projekt DEAL.

Conflict of Interest

The authors declare no conflict of interest.

Keywords

organic cathodes, polyimides, porous cathodes, potassium-ion batteries

Received: May 11, 2020

Revised: July 8, 2020

Published online:

[1] H. S. Zhou, *Energy Environ. Sci.* **2013**, *6*, 2256.

[2] N. Yabuuchi, K. Kubota, M. Dahbi, S. Komaba, *Chem. Rev.* **2014**, *114*, 11636.

- [3] H. Kim, J. C. Kim, M. Bianchini, D.-H. Seo, J. Rodriguez-Garcia, G. Ceder, *Adv. Energy Mater.* **2018**, *8*, 1702384.
- [4] J. C. Pramudita, D. Sehwat, D. Goonetilleke, N. Sharma, *Adv. Energy Mater.* **2017**, *7*, 1602911.
- [5] X. Wu, D. P. Leonard, X. Ji, *Chem. Mater.* **2017**, *29*, 5031.
- [6] A. Eftekhari, Z. Jian, X. Ji, *ACS Appl. Mater. Interfaces* **2017**, *9*, 4404.
- [7] W. B. Park, S. C. Han, C. Park, S. U. Hong, U. Han, S. P. Singh, Y. H. Jung, D. Ahn, K.-S. Sohn, M. Pyo, *Adv. Energy Mater.* **2018**, *8*, 1703099.
- [8] X. Wang, X. Xu, C. Niu, J. Meng, M. Huang, X. Liu, Z. Liu, L. Mai, *Nano Lett.* **2017**, *17*, 544.
- [9] Y.-H. Zhu, X. Yang, D. Bao, X.-F. Bie, T. Sun, S. Wang, Y.-S. Jiang, X.-B. Zhang, J.-M. Yan, Q. Jiang, *Joule* **2018**, *2*, 736.
- [10] C. Zhang, Y. Xu, M. Zhou, L. Liang, H. Dong, M. Wu, Y. Yang, Y. Lei, *Adv. Funct. Mater.* **2017**, *27*, 1604307.
- [11] A. Gao, M. Li, N. Guo, D. Qiu, Y. Li, S. Wang, X. Lu, F. Wang, R. Yang, *Adv. Energy Mater.* **2018**, *9*, 1802739.
- [12] H. Kim, J. C. Kim, S.-H. Bo, T. Shi, D.-H. Kwon, G. Ceder, *Adv. Energy Mater.* **2017**, *7*, 1700098.
- [13] L. Deng, X. Niu, G. Mo, Z. Yang, L. Zeng, Y. Zhu, L. Guo, *Adv. Funct. Mater.* **2018**, *28*, 1800670.
- [14] K. Chihara, A. Katogi, K. Kubota, S. Komaba, *Chem. Commun.* **2017**, *53*, 5208.
- [15] T. Deng, X. Fan, J. Chen, L. Chen, C. Luo, X. Zhou, J. Yang, S. Zheng, C. Wang, *Adv. Funct. Mater.* **2018**, *28*, 1800219.
- [16] J. Han, G. N. Li, F. Liu, M. Wang, Y. Zhang, L. Hu, C. Dai, M. Xu, *Chem. Commun.* **2017**, *53*, 1805.
- [17] Y. Tian, Y. An, S. Xiong, J. Feng, Y. Qian, *J. Mater. Chem. A* **2019**, *7*, 9716.
- [18] D. S. Charles, M. Feygenson, K. Page, J. Neufeind, W. Xu, X. Teng, *Nat. Commun.* **2017**, *8*, 15520.
- [19] Y. Hironaka, K. Kubota, S. Komaba, *Chem. Commun.* **2017**, *53*, 3693.
- [20] T. B. Schon, B. T. McAllister, P. F. Li, D. S. Seferos, *Chem. Soc. Rev.* **2016**, *45*, 6345.
- [21] Y. Xu, M. Zhou, Y. Lei, *Mater. Today* **2018**, *21*, 60.
- [22] C. Han, H. Li, R. Shi, T. Zhang, J. Tong, J. Li, B. Li, *J. Mater. Chem. A* **2019**, *7*, 23378.
- [23] Q. Zhao, Y. Lu, J. Chen, *Adv. Energy Mater.* **2017**, *7*, 1601792.
- [24] M. Lee, J. Hong, J. Lopez, Y. Sun, D. Feng, K. Lim, W. C. Chueh, M. F. Toney, Y. Cui, Z. Bao, *Nat. Energy* **2017**, *2*, 861.
- [25] Y. Lu, Q. Zhang, L. Li, Z. Niu, J. Chen, *Chem* **2018**, *4*, 2786.
- [26] J. Yang, Y. Shi, P. Sun, P. Xiong, Y. Xu, *ACS Appl. Mater. Interfaces* **2019**, *11*, 42305.
- [27] C. Zhang, Y. He, P. Mu, X. Wang, Q. He, Y. Chen, J. Zeng, F. Wang, Y. Xu, J.-X. Jiang, *Adv. Funct. Mater.* **2018**, *28*, 1705432.
- [28] C. Zhao, Z. Chen, W. Wang, P. Xiong, B. Li, M. Li, J. Yang, Y. Xu, *Angew. Chem., Int. Ed.* **2020**, *59*, 2.
- [29] Y. Chen, W. Luo, M. Carter, L. Zhou, J. Dai, K. Fu, S. Lacey, T. Li, J. Wan, X. Han, Y. Bao, L. Hu, *Nano Energy* **2015**, *18*, 205.
- [30] Z. Xing, Z. Jian, W. Luo, Y. Qi, C. Bommier, E. S. Chong, Z. Li, L. Hu, X. Ji, *Energy Storage Mater.* **2016**, *2*, 63.
- [31] Z. Jian, Y. Liang, I. A. Rodríguez-Pérez, Y. Yao, X. Ji, *Electrochem. Commun.* **2016**, *71*, 5.
- [32] Q. Zhao, J. Wang, Y. Lu, Y. Li, G. Liang, J. Chen, *Angew. Chem., Int. Ed.* **2016**, *55*, 12528.
- [33] L. Fang, R. Ma, J. Wang, H. Yang, B. Lu, *Adv. Mater.* **2018**, *30*, 1805486.
- [34] C. Zhang, Y. Qiao, P. Xiong, W. Ma, P. Bai, X. Wang, Q. Li, J. Zhao, Y. Xu, Y. Chen, J. H. Zeng, F. Wang, Y. Xu, J. X. Jiang, *ACS Nano* **2019**, *13*, 745.
- [35] B. Li, J. Zhao, Z. Zhang, C. Zhao, P. Sun, P. Bai, J. Yang, Z. Zhou, Y. Xu, *Adv. Funct. Mater.* **2018**, *29*, 1807137.
- [36] W. Deng, Y. Shen, J. Qian, H. Yang, *Chem. Commun.* **2015**, *51*, 5097.
- [37] X. Han, G. Qing, J. Sun, T. Sun, *Angew. Chem., Int. Ed.* **2012**, *51*, 5147.
- [38] Y. Shi, H. Tang, S. Jiang, L. V. Kayser, M. Li, F. Liu, F. Ji, D. J. Lipomi, S. P. Ong, Z. Chen, *Chem. Mater.* **2018**, *30*, 3508.
- [39] H. Wang, S. Yuan, D. Ma, X. Huang, F. Meng, X. Zhang, *Adv. Energy Mater.* **2014**, *4*, 1301651.
- [40] J. Wang, F. Li, Y. Qu, Y. Liu, Y. Yang, W. Li, M. Zhao, *J. Mater. Chem. A* **2018**, *6*, 24869.
- [41] X. Fan, F. Wang, X. Ji, R. Wang, T. Gao, S. Hou, J. Chen, T. Li, X. Deng, L. Chen, C. Luo, L. Wang, C. Wang, *Angew. Chem., Int. Ed.* **2018**, *57*, 7146.
- [42] C. Wang, Y. Fang, Y. Xu, L. Liang, M. Zhou, H. Zhao, Y. Lei, *Adv. Funct. Mater.* **2016**, *26*, 1777.
- [43] V. Augustyn, J. Come, M. A. Lowe, J. W. Kim, P. L. Taberna, S. H. Tolbert, H. D. Abruna, P. Simon, B. Dunn, *Nat. Mater.* **2013**, *12*, 518.
- [44] Y. Xu, C. Zhang, M. Zhou, Q. Fu, C. Zhao, M. Wu, Y. Lei, *Nat. Commun.* **2018**, *9*, 1720.
- [45] L. Fan, Q. Liu, Z. Xu, B. Lu, *ACS. Energy Lett.* **2017**, *2*, 1614.
- [46] J. Liao, Q. Hu, Y. Yu, H. Wang, Z. Tang, Z. Wen, C. Chen, *J. Mater. Chem. A* **2017**, *5*, 19017.
- [47] T. Deng, X. Fan, C. Luo, J. Chen, L. Chen, S. Hou, N. Eidson, X. Zhou, C. Wang, *Nano Lett.* **2018**, *18*, 1522.
- [48] K. Moyer, J. Donohue, N. Ramanna, A. P. Cohn, N. Muralidharan, J. Eaves, C. L. Pint, *Nanoscale* **2018**, *10*, 13335.
- [49] J. Ding, H. Wang, Z. Li, K. Cui, D. Karpuzov, X. Tan, A. Kohandehghan, D. Mitlin, *Energy Environ. Sci.* **2015**, *8*, 941.
- [50] R. Thangavel, A. G. Kannan, R. Ponraj, M.-S. Park, H. Choi, D.-W. Kim, Y.-S. Lee, *Adv. Mater. Interfaces* **2018**, *5*, 1800472.
- [51] H. Li, L. Peng, Y. Zhu, X. Zhang, G. Yu, *Nano Lett.* **2016**, *16*, 5938.